Plug-In Hybrid Electric Vehicles: Replacing Internal Combustion Engine With Clean and Renewable Energy Based Auxiliary Power Sources

Hassan Fathabadi

***Abstract*—A plug-in hybrid electric vehicle (PHEV) uses an internal combustion engine to extend its cruising range, and to produce the electric power needed to be supplied to its electric motor when the charge level of the vehicle's battery becomes low and reaches a predetermined state of charge (SOC). This paper provides a better solution by replacing the internal combustion engine of a PHEV with a small-size photovoltaic (PV) module located on the roof of the PHEV, and a micro wind turbine located in front of the PHEV, behind the condenser of the air conditioning system. Thus, this study proposes a novel battery/PV/wind hybrid power source to be utilized in PHEVs. The power source equipped with vehicle-to-grid (V2G) technology is composed of a 19.2-kWh Lithium (Li)-ion battery used as the main energy storage device, and a PV module and a wind energy conversion system. A prototype of the battery/PV/wind hybrid power source has been constructed and utilized in a PHEV. Experimental verifications are presented that demonstrate utilizing the PV module and micro wind turbine adds 19.6 km to the cruising range of a PHEV with the weight of 1880 kg during two sunny days, and provides higher power efficiency (91.2%) and speed (121 km/h). Highly accurate dc-link voltage regulation and producing an appropriate three-phase stator current for the traction motor by using pulse width modulation technique are the other contributions of this paper.**

***Index Terms*—Lithium-ion battery, micro wind turbine, photovoltaic (PV), plug-in hybrid electric vehicle (PHEV).**

NOMENCLATURE

C_1	Parasitic capacitance of the N-MOSFET switch of the two converters connected to the PV module and WECS (F).
C_2	Secondary-side capacitor of the two converters connected to the photovoltaic (PV) module and wind energy conversion system (WECS) (F).
$C_{\rm pv}$	Input capacitor of the converter connected to the PV module (F).
$C_{\rm we}$	Input capacitor of the converter connected to the WECS (F).
$C_{\rm dc}$	DC-link capacitor (F).
$D_{\rm char}$	Duty cycle of the signal supplied to the converter connected to the Li-ion battery in charging mode.
$D_{\rm disc}$	Duty cycle of the signal supplied to the converter connected to the battery in discharging mode.
$D_{\rm pv}$	Duty cycle of the converter connected to the PV module.
D_S	Duty cycle of the switching pulse supplied to the switch N-MOSFET S_1.
$D_{\rm we}$	Duty cycle of the converter connected to the WECS.
f_s	Constant switching frequency of the two converters connected to the PV module and WECS (Hz).
G	Solar irradiance on the PV module ($\mathrm{W}\cdot\mathrm{m}^{-2}$).
$I_{\rm bat}$	Li-ion battery output current (A).
$I_{\rm load}$	Load current supplied to the three-phase inverter and traction motor (A).
$I_{\rm pv}$	PV module output current (A).
$I_{\rm pv-mpp}$	PV module current at maximum power point (A).
$I_{\rm we}$	WECS output current (A).
$n = N_2/N_1$	Turns ratio of the two transformers of the two converters connected to the PV module and WECS.
$P_{\rm pv}$	PV module output power (W).
$P_{\rm char}$	Charging power of the Li-ion battery (W).
$P_{\rm dischar}$	Discharging power of the Li-ion battery (W).
$P_{\rm load}$	Total electric power supplied to the three-phase inverter and traction motor (W).
$P_{\rm pv-mpp}$	PV module power at maximum power point (W).
$P_{\rm we}$	WECS output power (W).
$R_{\rm bat-esr}$	Equivalent series resistance (ESR) of the Li-ion battery (Ω).
$R_{\rm esr}$	ESR of the dc-link capacitor (Ω).
$R_{\rm in}$	Input resistance of the converter connected to the PV module (Ω).
R_L	Equivalent resistance of the output terminal of the converter connected to the PV module (Ω).
$R_{L_{\rm bat}}$	Resistance of the inductor $L_{\rm bat}$ of the bidirectional boost-buck converter connected to the Li-ion battery (Ω).
$S_{\rm pv}$	N-MOSFET switch used in the converter connected to the PV module.
$S_{\rm we}$	N-MOSFET switch of the converter connected to the WECS.

Manuscript received August 10, 2017; revised November 21, 2017; accepted January 10, 2018. Date of publication January 24, 2018; date of current version August 7, 2018. Recommended for publication by Associate Editor Prof. Wenping Cao.

The author is with the National Technical University of Athens, Athens 10682, Greece (e-mail: h4477@hotmail.com).

Color versions of one or more of the figures in this paper are available online at http://ieeexplore.ieee.org.

Digital Object Identifier 10.1109/TPEL.2018.2797250

T	PV module temperature (°C).
T_s	Switching period of the two converters connected to the PV module and WECS (sec).
T_b	Switching period of the control signal supplied to the converter connected to the Li-ion battery (sec).
$V_{\rm bat}$	Li-ion battery output voltage (V).
$V_{\rm dc}$	DC-link voltage (V).
$V_{\rm in}$	Input voltage of the converter (V).
$V_{\rm pv}$	PV module output voltage (V).
$V_{\rm pv-mpp}$	PV module voltage at maximum power point (V).
$V_{\rm we}$	WECS output voltage (V).
α	Power efficiency of the converter connected to the PV module.
β	Power efficiency of the converter connected to the WECS.

I. Introduction

BECAUSE of environmental issues and economic considerations, there is an upward trend in developing the usage of electric vehicles (EVs), hybrid electric vehicle (HEV) and plug-in hybrid electric vehicles (PHEVs) rather than the vehicles with internal combustion engines [1], [2], so there is an ascending demand for different types of EV charging stations in some countries [3], [4]. A PHEV utilizes its electric motor to provide the power needed for propulsion, and is more efficient compared to a traditional HEV that mainly uses an internal combustion engine [5]. The vehicle-to-grid (V2G) technology implemented in PHEVs is the other benefit that makes them more advantageous and popular [6], [7]. In particular, the advantage of a PHEV is highlighted when it is connected to a microgrid or a smart grid to manage and balance load demand [8], [9]. A through survey of the current literature shows that the research works concerning PHEVs can be classified into the three categories. The first category includes the researches performed to improve the performance of the batteries used in PHEVs. For instance, an analysis about the battery aging in a PHEV by using the experimental data about the voltage recovery and internal resistance of the battery was reported in [10]. Some other related works are analyzing the effect of thermal management on PHEVs' batteries [11], determining a suitable Li-ion battery pack for a PHEV [12], evaluating the impact of ultracapacitors on degradation of the performance of a Li-ion battery used in a PHEV [13], and maximization of the income of charging the batteries of PHEVs [14]. The second category is composed of the research works that have proposed some peripheral devices and facilities for PHEVs such as the wireless charging mechanism applicable to PHEVs [15], and the resonant converter based battery charger suitable for a PHEV [16]. Finally, the third category comprises the articles that propose different strategies to combine the charging and discharging process of PHEVs with other power sources such as renewable energy resources to satisfy load demand in a grid [17]. Some examples are utilizing PHEVs in a smart grid to optimize the electrical parameters of the grid by providing distributed demand response [18], and new energy management scheme proposed for utilizing solar energy in PHEVs [19].

The main drawback of a PHEV is that it uses an internal combustion engine to extend its cruising range, and to produce the electric power needed to be supplied to its electric motor when the charge level of the vehicle's battery becomes low and gets to a predetermined state of charge (SOC). This study addresses this problem by presenting a novel battery/PV/wind hybrid power source utilized in a PHEV with the weight of 1880 kg. The rest of this paper is organized as follows. The proposed battery/PV/wind hybrid power source is designed and implemented in Section II. Details about the constructed hybrid power source and experimental verifications are given in Section III, and the paper is concluded in Section IV.

II. Implementation of the Battery/PV/Wind Hybrid Power Source Proposed for PHEVs

The configuration of the battery/PV/wind hybrid power source proposed to be utilized in PHEVs is shown in Fig. 1. It is composed of a Li-ion rechargeable battery used as the main energy storage device, a bidirectional dc/dc boost–buck converter connected to the Li-ion battery, a single-phase bidirectional dc/ac inverter connected between the battery and grid to provide V2G operation, a PV module used as the auxiliary power source, a unidirectional dc/dc boost converter connected to the PV module, a wind energy conversion system (WECS) used as the other auxiliary power source, a unidirectional dc/dc boost converter connected to the WECS, a three-phase bidirectional pulse width modulation (PWM) dc/ac inverter connected the traction motor, which is practically a three-phase permanent magnet synchronous motor (PMSM), and a combined power control and maximum power point tracking (MPPT) unit. It is reminded that in a PV system, the MPPT unit tracks the maximum power point (MPP) of the PV module connected to the system [20]. The WECS itself consists of a micro wind turbine, a permanent magnet synchronous generator (PMSG), and a three-phase rectifier. The dc-link voltage is continuously regulated to a designated constant value. Fig. 2 shows the electric circuit of the two similar unidirectional dc/dc boost converters connected to the PV module and WECS. The converter provides an average power efficiency of 98% around its nominal operating point referring to a power transmission of 200 W, and its gain is given as [21]

$$\frac{V_{\rm dc}}{V_{\rm in}} = \frac{n}{1 - D_S} \tag{1}$$

so, the dc-link voltage is given as

$$V_{\rm dc} = \frac{nV_{\rm we}}{1 - D_{\rm we}}. \tag{2}$$

Equation (2) demonstrates that the dc-link voltage is continuously regulated to a designated constant value by varying the duty cycle $D_{\rm we}$. As shown in Fig. 1, the output current ($I_{\rm we}$) and voltage ($V_{\rm we}$) of the WECS, and hence, the WECS output power ($P_{\rm we}$) is continually calculated by the power control unit as

$$P_{\rm we} = V_{\rm we} I_{\rm we}. \tag{3}$$

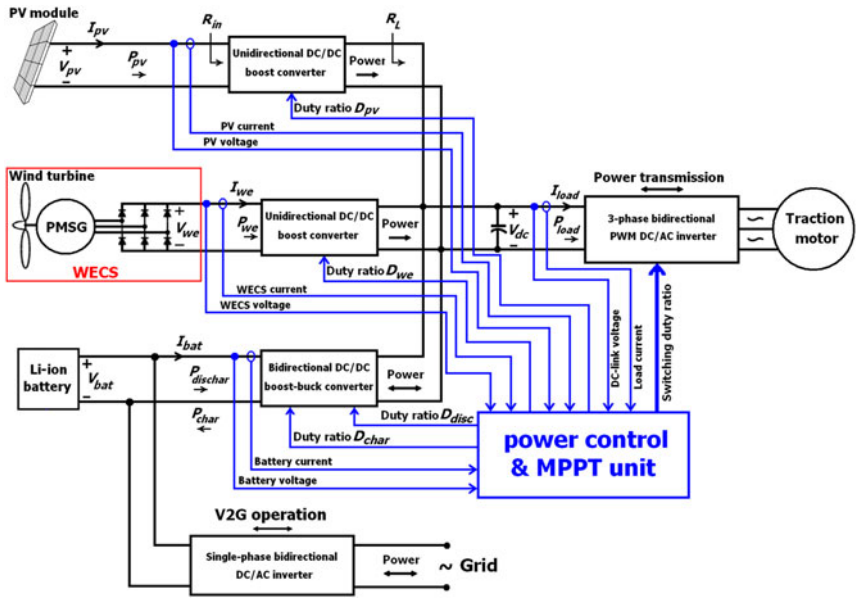

Fig. 1. Configuration of the battery/PV/wind hybrid power source proposed to be utilized in PHEVs.

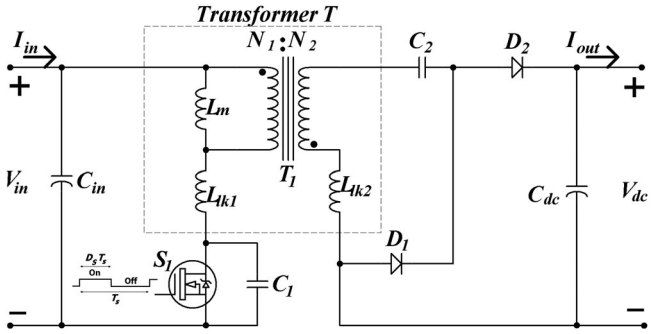

Fig. 2. Unidirectional dc/dc boost converter connected to the PV module and WESC.

The PV voltage is given as

$$V_{\rm pv} = \frac{(1 - D_{\rm pv})V_{\rm dc}}{n}. \tag{4}$$

As mentioned above, the dc-link voltage is a constant value, so in accordance with (4), the MPPT unit continuously tunes the duty cycle $D_{\rm pv}$ to regulate the voltage of the PV module ($V_{\rm pv}$) to the voltage at MPP ($V_{\rm pv-mpp}$). In detail, when $V_{\rm pv}$ is less than $V_{\rm pv-mpp}$, the MPPT unit decreases the duty cycle $D_{\rm pv}$, and contrarily, the duty cycle $D_{\rm pv}$ is increased by the MPPT unit when $V_{\rm pv}$ is more than $V_{\rm pv-mpp}$. The other way to clearly explain the theoretical concept of the MPPT process is the functional association between the output power of the PV module and the duty cycle $D_{\rm pv}$ that is formulized in detail as

$$P_{\rm pv} = V_{\rm pv} I_{\rm pv} = \frac{{V_{\rm pv}}^2}{R_{\rm in}} \approx \frac{{V_{\rm pv}}^2}{\frac{(1-D_{\rm pv})^2}{n^2} R_L} \tag{5}$$

where $R_{\rm in}$ and R_L introduced in the Nomenclature section are shown in Fig. 1. Equation (5) explicitly demonstrates that the PV output power can be regulated to its maximum amount, i.e., the PV power at MPP ($P_{\rm pv-mpp}$) by varying the duty cycle $D_{\rm pv}$. As shown in Fig. 1, the PV module output current and voltage,

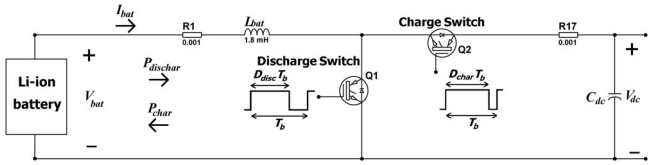

Fig. 3. Bidirectional dc/dc boost–buck converter connected to the Li-ion battery.

and hence, the PV output power is continually calculated by the power control unit. In each step, the calculated power is compared to the previous amount to find the maximum available power by varying the duty cycle $D_{\rm pv}$. The electric circuit of the bidirectional dc/dc boost–buck converter with the average power efficiency of 90% connected to the Li-ion battery is shown in Fig. 3. The discharging power of the Li-ion battery is given as

$$P_{\rm dischar} = V_{\rm bat} I_{\rm bat}. \tag{6}$$

The Li-ion battery output voltage and current ($V_{\rm bat}$ and $I_{\rm bat}$), and hence, the discharging and charging powers of the Li-ion battery are continuously calculated by the power control unit as shown in Fig. 1. Noting Fig. 3 demonstrates that in discharging mode, the converter operates as a boost converter, and the discharging power of the Li-ion battery is expressed as

$$P_{\rm dischar} = \frac{1}{0.9}\left[\left(\frac{1}{1-D_{\rm disc}}\right) V_{\rm bat} \left(\frac{\left(\frac{1}{1-D_{\rm disc}}\right) V_{\rm bat} - V_{\rm dc}}{0.001 + R_{\rm esr}}\right)\right] \tag{7}$$

where $D_{\rm disc}$ is the duty cycle of the control signal supplied to the gate of the insulated gate bipolar transistor (IGBT) Q1 (discharge switch) as shown in Fig. 3. It is deduced from (7) that the discharging power can be regulated to a required power rate by varying the duty cycle $D_{\rm disc}$. In charging mode, the direction of the battery current becomes reverse, the converter operates

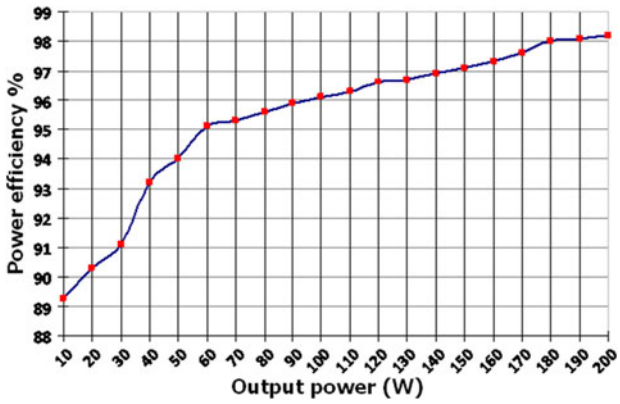

Fig. 4. Experimental result: Power efficiency of the unidirectional dc/dc boost converter versus its output power.

as a buck converter, and the charging power is found as

$$P_{\rm char} = D_{\rm char} V_{\rm dc} \left(\frac{D_{\rm char} V_{\rm dc} - V_{\rm bat}}{0.001 + R_{\rm bat-esr} + R_{L_{\rm bat}}} \right) \tag{8}$$

where $D_{\rm char}$ is the duty cycle of the switching pulse supplied to the gate of the IGBT Q2 (charge switch) as shown in Fig. 3. Thus, in a similar manner, the charging power is regulated to a required power rate by varying the duty cycle $D_{\rm char}$. As shown in Fig. 1, the power control unit also measures the dc-link voltage ($V_{\rm dc}$) and load current ($I_{\rm load}$), and then computes the total electric power ($P_{\rm load}$) supplied to the three-phase bidirectional PWM dc/ac inverter and the three-phase traction motor connected to the inverter as

$$P_{\rm load} = V_{\rm dc} I_{\rm load} \tag{9}$$

Experimental curve indicating the power efficiency of the two similar unidirectional dc/dc boost converters connected to the PV module and WECS is shown in Fig. 4. In the experimental curve, the red points (data) have been used to program the microcontroller. At any time, the microcontroller estimates the power efficiencies (α and β) of the two converters by comparing these data with the calculated PV and WECS output powers ($P_{\rm pv}$ and $P_{\rm we}$). The power control in the battery/PV/wind hybrid power source is performed by the power control unit as below

Case 1 (charging mode): If $\alpha P_{\rm pv} + \beta P_{\rm we} \geq P_{\rm load}$, then the power control unit sets the Li-ion battery in charging mode by activating the duty cycle $D_{\rm char}$ as shown in Figs. 1 and 3. In this case, the power balance in the hybrid power source is expressed as

$$\alpha P_{\rm pv} + \beta P_{\rm we} = P_{\rm load} + \frac{1}{0.9} P_{\rm char}. \tag{10}$$

So, the electric power consumed to charge the Li-ion battery is obtained as

$$P_{\rm char} = 0.9 \left(\alpha P_{\rm pv} + \beta P_{\rm we} - P_{\rm load} \right). \tag{11}$$

It is derived from comparing (8) with (11) that

$$D_{\rm char} V_{\rm dc} \left(\frac{D_{\rm char} V_{\rm dc} - V_{\rm bat}}{0.001 + R_{\rm bat-esr} + R_{L_{\rm bat}}} \right) = 0.9 \left(\alpha P_{\rm pv} + \beta P_{\rm we} - P_{\rm load} \right). \tag{12}$$

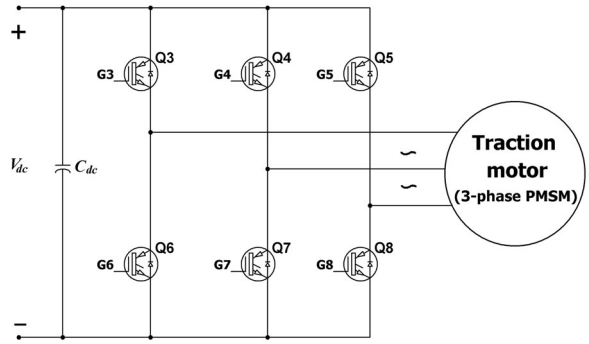

Fig. 5. Three-phase bidirectional PWM six-switch dc/ac inverter.

Equation (12) explicitly demonstrates that in this case (charging mode), the power control unit measures $P_{\rm pv}$, $P_{\rm we}$, and $P_{\rm load}$, and then regulates the charging power of the Li-ion battery to the required amount specified in (11) by varying $D_{\rm char}$.

Case 2 (discharging mode): If $\alpha P_{\rm pv} + \beta P_{\rm we} < P_{\rm load}$, then the power control unit sets the Li-ion battery in discharging mode by activating the duty cycle $D_{\rm disc}$ as shown in Figs. 1 and 3 to provide the additional electric power needed. In this case, the power balance in the hybrid power source is expressed as

$$\alpha P_{\rm pv} + \beta P_{\rm we} + 0.9 P_{\rm dischar} = P_{\rm load}. \tag{13}$$

In this case, the amount of the supplementary electric power that should be provided by discharging the Li-ion battery is found from (13) as

$$P_{\rm dischar} = \frac{1}{0.9} \left(P_{\rm load} - \alpha P_{\rm pv} - \beta P_{\rm we} \right). \tag{14}$$

By replacing $P_{\rm dischar}$ from (7) in (14), it is found that

$$\left(\frac{1}{1 - D_{\rm disc}} \right) V_{\rm bat} \left(\frac{\left(\frac{1}{1 - D_{\rm disc}} \right) V_{\rm bat} - V_{\rm dc}}{0.001 + R_{\rm esr}} \right) = P_{\rm load} - \alpha P_{\rm pv} - \beta P_{\rm we}. \tag{15}$$

It is deduced from (15) that in this case (discharging mode), the power control unit measures $P_{\rm pv}$, $P_{\rm we}$, and $P_{\rm load}$, and then regulates the discharging power of the Li-ion battery to the amount demanded in (14) by varying $D_{\rm disc}$. It can be summarized that each duty cycle controls only one parameter with the following systematic control sequence:

$$\begin{aligned} &1)\ D_{\rm we} \rightarrow V_{\rm dc}; \\ &2)\ D_{\rm pv} \rightarrow P_{\rm pv}; \\ &3)\ D_{\rm char} \rightarrow P_{\rm char} \quad \text{or} \quad D_{\rm disc} \rightarrow P_{\rm dischar}. \end{aligned} \tag{16}$$

There is no interact between the four duty cycles ($D_{\rm we}$, $D_{\rm pv}$, $D_{\rm char}$, and $D_{\rm disc}$), which are the control variables. Similarly, there is no interact between the four controlled parameters ($V_{\rm dc}$, $P_{\rm pv}$, $P_{\rm char}$, and $P_{\rm dischar}$). The only limitation is that $V_{\rm dc}$ is first regulated by varying the duty cycle $D_{\rm we}$, and then, $P_{\rm pv}$ is regulated by varying the duty cycle $D_{\rm pv}$, and finally, $P_{\rm char}$ or $P_{\rm dischar}$ is regulated by, respectively, varying the duty cycle $D_{\rm char}$ or $D_{\rm disc}$. The electric circuit of the proposed three-phase bidirectional PWM six-switch dc/ac inverter connected the traction motor is shown in Fig. 5. It comprises the six IGBTs that

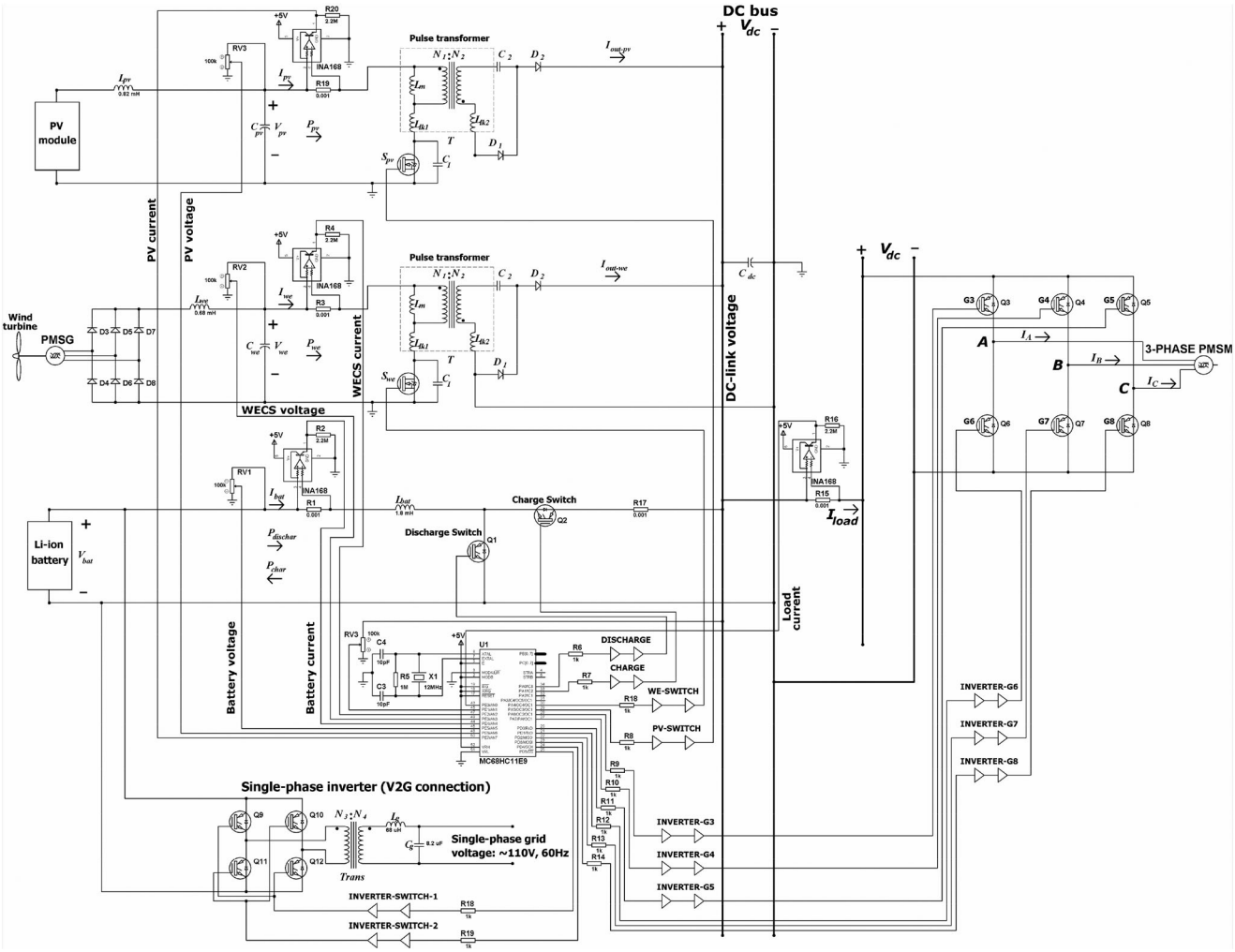

Fig. 6. Electric circuit of the constructed battery/PV/wind hybrid power source.

convert the dc-link voltage into a three-phase three-level PWM ac voltage supplied to the stator of the traction motor, which is in practice a three-phase PMSM. The traction motor acts as a three-phase inductive load, so the current supplied to the stator is the integral of the three-level PWM ac voltage produced by the inverter. Since the three-phase three-level PWM ac voltage is different from a three-phase sinusoidal voltage, the current waveform is inevitably close to a sinusoidal form, not entirely sinusoidal form, and this means distortion occurs in the current waveform. As shown in Fig. 5, each IGBT itself includes an emitter-to-collector connected diode, the six diodes operate as a three-phase rectifier to convert the three-phase ac voltage resulted from the regenerative power produced by the traction motor during decelerating and braking into the dc-link voltage to be used to charge the Li-ion battery.

III. Construction of the Battery/PV/Wind Hybrid Power Source and Experimental Verifications

The configuration of the proposed battery/PV/wind hybrid power source was shown in Fig. 1, based on which the power source has been constructed to provide experimental verifications. The electric circuit of the constructed battery/PV/wind hybrid power source is shown in Fig. 6. As shown in Fig. 6, the microcontroller MC68HC11E9 has been used as the power control and MPPT unit. The detailed specifications of all the components used to construct the battery/PV/wind hybrid power source proposed to be utilized in PHEVs are listed in Table I. An 80-kW three-phase PMSM used as the traction motor, a 19.2-kWh Li-ion battery, a PV module KC200GT, a 100-W micro wind turbine and a 100-W PMSG connected to the micro wind turbine have been utilized. Fig. 7 shows the photographs of the PHEV equipped with the proposed battery/PV/wind hybrid power source, the PV module positioned on the roof of the PHEV, the micro wind turbine, and the PMSG connected to the micro wind turbine. The waveforms of the line voltages ($V_{\rm AB}$ and $V_{\rm BC}$) supplied to the PMSM and the dc-link voltage are shown in Fig. 8. The waveforms of the line voltages show that they are the three-level ac voltages with correct magnitude and phase produced using PWM technique by the three-phase bidirectional dc/ac inverter, and this explicitly verifies the correct operation of the three-phase bidirectional PWM six-switch dc/ac inverter connected to the traction motor. Similarly, the waveform of the dc-link voltage explicitly demonstrates that

TABLE I
TECHNICAL SPECIFICATION OF THE COMPONENTS USED IN THE CONSTRUCTED HYBRID POWER SOURCE UTILIZED IN A PHEV WITH THE WEIGHT OF 1880 KG

Traction motor		**Two DC/DC boost converters connected to PV module and WECS**	
Model	LSRPM 200 L	C_{pv} & C_{we} (μF)-Aluminum electrolytic capacitor/400 V	470
Made by	Leroy-Somer Co.	Converter switching frequency: f_s (kHz)	25
Type	Permanent magnet synchronous motor (PMSM)	DC-link voltage V_{dc} (V)	400
Phase number	3	DC-link capacitor C_{dc} (μF)-Aluminum electrolytic capacitor/600 V	680
Nominal line voltage (V)	400	Average ESR of C_{dc}: R_{esr} (mΩ)	109
Rated power (kW)	80	C_2 (μF)-Premium metallized polypropylene capacitor/600 V	22
Rated torque (Nm)	170	C_1 (nF)-Parasitic capacitance of IRFPS40N60K	1.2
Rated current (A)	157	Type of transformer T	Pulse
Speed range (rpm)	0-4500	$n = N_2/N_1$	$20/3$
Efficiency (%)	95.7	MOSFET switch S_{pv} & S_{we}	IRFPS40N60K
Maximum torque/Rated torque	1.4	Diodes: D_1-D_2	15ETH06S
Magnet material	NdFeB	**PV module KC200GT**	
Maximum current/Rated current	1.5	Current at MPP I_{pv-mpp} (A)	7.61
Moment of inertia (kg.m^2)	0.15	Voltage at MPP V_{pv-mpp} (V)	26.3
Weight (kg)	145	Output power at MPP P_{pv-mpp} (W)	200.1430
Battery bank: Sixteen 12 V/100 Ah Li-ion batteries		Short-circuit current I_{sc} (A)	8.21
Type	Li-ion	Open-circuit voltage V_{oc} (V)	32.9
Voltage (V)	48	**DC/DC converter connected to the Li-ion battery bank**	
Current capacity (Ah)	400	Type	Bidirectional boost-buck
Capacity (kWh)	19.2	IGBT switches: SW, Q1-Q2	STGY40NC60VD ×40
Series-connected batteries	4	$R_{t_{bat}}$ (mΩ)	10.8
Parallel-connected sets	4	**Single-phase inverter (V2G connection)** (Single-phase grid voltage: ~110 VAC, 60 Hz)	
Average ESR ($R_{bat-esr}$ (mΩ))	2.9	IGBT switches: Q9-Q12	STGY40NC60VD ×8
Permanent magnet synchronous generator (PMSG)		N_4/N_3	$39/12$
Model	PMG-100	L_g (μH)	68
Type	Three-phase, star connection	C_g (μF)	8.2
Rated power (W)	100	**Micro wind turbine**	
Maximum power	130	Rated power (W)	100
Rated phase voltage (V)	12	Rated wind speed (m/s)	10
Rated rotation (rpm)	690	Size: diameter (cm)	76
Magnet material	NdFeB	**Three-phase bidirectional PWM six-switch DC/AC inverter**	
Weight (kg)	2.8	IGBT switches: Q3-Q8	STGY40NC60VD ×5

the dc-link voltage is exactly regulated to the appointed value (400 V). The waveforms of the currents (I_A and I_B) supplied to the stator of the PMSM are shown in Fig. 9. The periodic switching pulse with the switching frequency of 25 kHz and the duty cycle $D_{\rm pv}$, the regulated dc-link voltage and PV output voltage are shown in Fig. 10. As mentioned above, the periodic switching pulse is produced by the microcontroller, and then, is supplied to the switch $S_{\rm pv}$ of the unidirectional dc/dc boost converter connected to the PV module. Fig. 10 demonstrates that the duty cycle of the switching pulse supplied to the converter connected to the PV module is about 0.562 ($D_{\rm pv} = 0.562$), $V_{\rm dc} = 400\,{\rm V}$, and $V_{\rm pv} = 26.25\,{\rm V}$. Considering the parameters

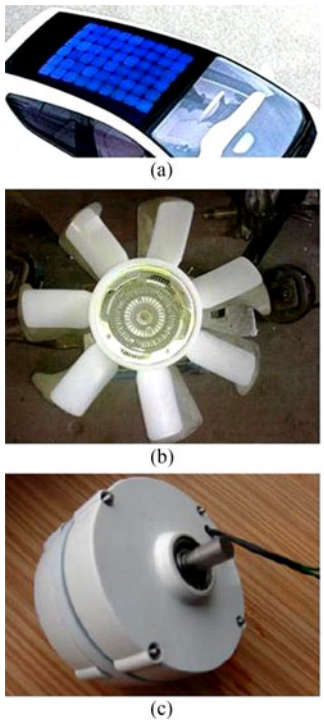

Fig. 7. PHEV equipped with the hybrid power source: (a) PV module positioned on the roof of the PHEV. (b) Micro wind turbine. (c) PMSG.

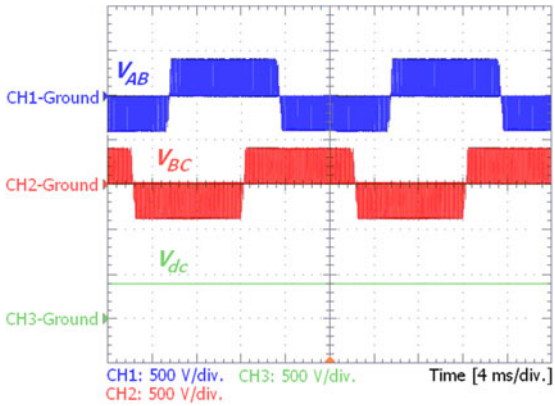

Fig. 8. Waveforms of the line voltages supplied to the PMSM, and the regulated dc-link voltage.

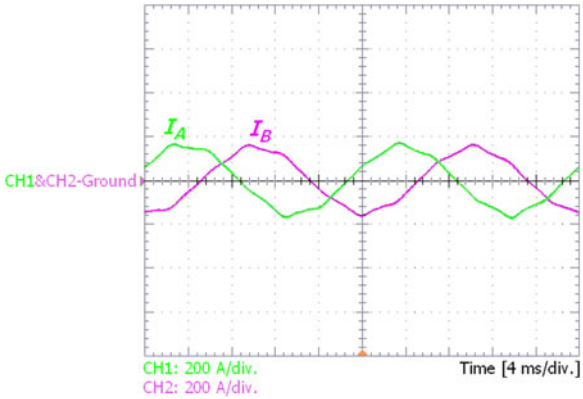

Fig. 9. Waveforms of the currents supplied to the stator of the PMSM.

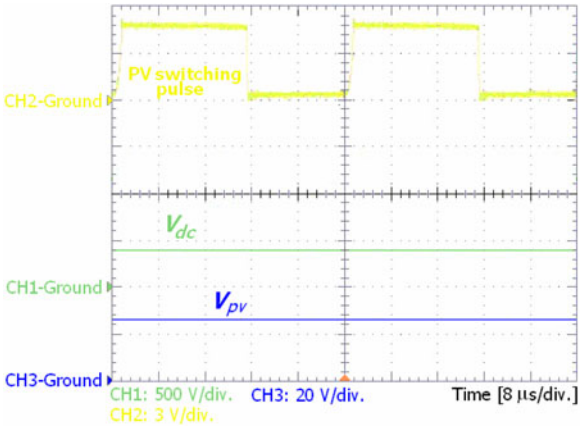

Fig. 10. Periodic switching pulse supplied to the switch of the dc/dc converter, the dc-link voltage and the operating voltage of the PV module.

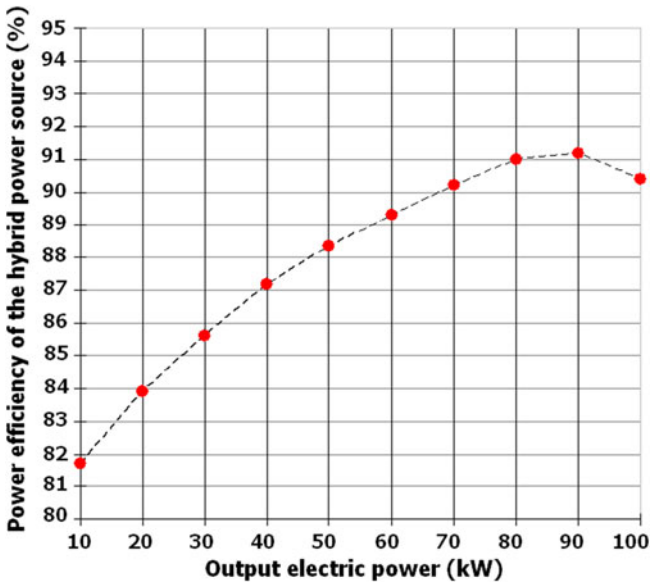

Fig. 11. Power efficiency of the battery/PV/wind hybrid power proposed to be utilized in PHEVs.

of the converter reported in Table I ($n = 20/3$), these values are exactly compatible with (4). Comparing the operating voltage of the PV module (26.25 V) to the MPP voltage of the PV module ($V_{\mathrm{pv-mpp}} = 26.3\,\mathrm{V}$) under nominal condition (solar irradiance $G = 1000\,\mathrm{W}\cdot\,\mathrm{m}^{-2}$, temperature $T = 25\,^{\circ}\mathrm{C}$) reported in Table I explicitly verifies that the MPPT unit highly accurately tracks the MPP of the PV module. The electric power supplied to the traction motor (PMSM) and the total of the electric power produced by the PV module, WECS, and discharging the Li-ion battery were measured point by point, and then, the power efficiency of the proposed battery/PV/wind hybrid power source was obtained point by point as shown in Fig. 11. The following points, which are the main contributions of this study are deduced from the experimental results shown in Figs. 8–11:

1) The power efficiency curve explicitly demonstrates that the proposed battery/PV/wind hybrid power source provides a maximum power efficiency of 91.2% around the rated power of the traction motor.

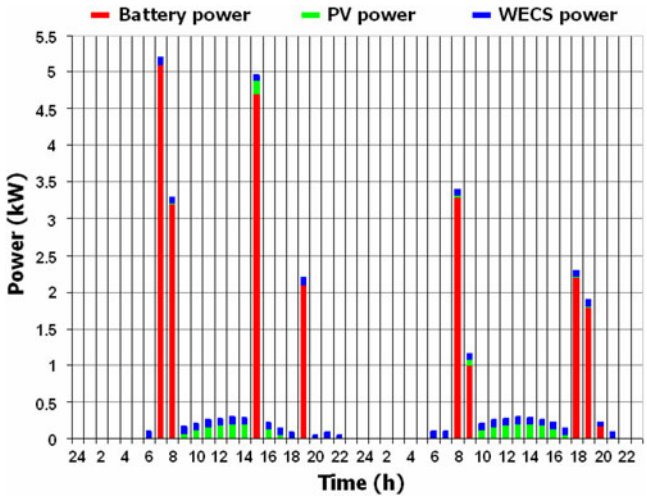

Fig. 12. Power flow measured hour by hour during two days.

TABLE II
COMPARISON BETWEEN THE TECHNICAL PARAMETERS OF THE HYBRID BATTERY/PV/WIND POWER SOURCE IN DIFFERENT MODES

Mode of the power source	Analysis type	Cruising range (km)	Max. speed (km/h)	0-100 km/h acceleration (sec)	Max. efficiency (%)	PHEV weight (kg)
Battery/PV/wind	Experiment	**129.6**	**121**	13.4	**91.2**	1880
Battery/PV	Experiment	**123.4**	**121**	13.4	**91.1**	1880
Battery/wind	Experiment	**116.3**	120	13.4	**90.4**	1880
Battery	Experiment	110	120	13.4	90.2	1880

2) The dc-link voltage is high accurately regulated to the appointed value (400 V).
3) The traction motor is well supplied by the sinusoidal currents resulted from the three-level ac voltages produced by using PWM technique.

The hybrid power source was utilized in a PHEV with the weight of 1880 kg, and to evaluate the impact of the PV module and WECS, four experiments were performed. In the first experiment, the PV module and WECS both were in operation, so the power source was in battery/PV/wind hybrid mode. The power flow representing the power provided by the battery, PV module, and WECS is shown in detail in Fig. 12.

In the second experiment, the WECS was isolated from the system, so the power source was in battery/PV hybrid mode.

Similarly, the PV module was isolated from the system in the third experiment, so the power source was in battery/wind hybrid mode. Finally, in the fourth experiment, the PV module and WECS both were isolated from the system, and so the power source was in battery mode. The results of the four experiments are summarized in Table II, the experimental results demonstrate that utilizing the PV module and micro wind turbine adds 19.6 km to the cruising range of the PHEV during two sunny days, and provides higher power efficiency (91.2%) and speed (121 km/h). As reported in Table II, a PHEV with the weight of 1880 kg equipped with the proposed battery/PV/wind hybrid power source has a maximum speed of 121 km/h and a cruising range of 129.6 km.

The construction cost of the PV system and WECS implemented in the PHEV is about €850, while the internal combustion engine replaced with the proposed PV/wind power source

costs €3100. Moreover, the internal combustion engine should be supplied with gasoline, which is expensive in many countries, while the PV/wind power source implemented as a replacement uses solar and wind energy as renewable energy free of any charge.

IV. Conclusion

In this paper, a novel battery/PV/wind hybrid power source was proposed to replace the gasoline-powered internal combustion engine of a PHEV with a small-size PV module located on the roof of the PHEV, and a micro wind turbine located in front of the PHEV, behind the condenser of the air conditioning system. The power source has the capability of V2G, and utilizes a 19.2-kWh Li-ion battery as the main energy storage device, and a PV module and a WECS including the micro wind turbine as the auxiliary power sources. A prototype of the battery/PV/wind hybrid power source has been built and utilized in a PHEV. The experimental verifications were presented that demonstrated utilizing the PV module and micro wind turbine adds 19.6 km to the cruising range of a PHEV with the weight of 1880 kg during two sunny days, and provides higher power efficiency (91.2%) and speed (121 km/h). It was also shown that the power source high accurately regulates the dc-link voltage, and produces suitable stator currents for the traction motor by using PWM technique.

References

[1] N. Adnan, S. M. Nordin, and I. Rahman, "Adoption of PHEV/EV in Malaysia: A critical review on predicting consumer behaviour," *Renew. Sustain. Energy Rev.*, vol. 72, pp. 849–862, 2017.

[2] H. Fathabadi, "Utilization of electric vehicles and renewable energy sources used as distributed generators for improving characteristics of electric power distribution systems," *Energy*, vol. 90, pp. 1100–1110, 2015.

[3] H. Fathabadi, "Novel grid-connected solar/wind powered electric vehicle charging station with vehicle-to-grid technology," *Energy*, vol. 132, pp. 1–11, 2017.

[4] D. Q. Hung, Z. Y. Dong, and H. Trinh, "Determining the size of PHEV charging stations powered by commercial grid-integrated PV systems considering reactive power support," *Appl. Energy*, vol. 183, pp. 160–169, 2016.

[5] H. Fathabadi, "Novel solar powered electric vehicle charging station with the capability of vehicle-to-grid," *Solar Energy*, vol. 142, pp. 136–143, 2017.

[6] M. C. Kisacikoglu, B. Ozpineci, and L. M. Tolbert, "EV/PHEV bidirectional charger assessment for V2G reactive power operation," *IEEE Trans. Power Electron.*, vol. 28, no. 12, pp. 5717–5727, 2013.

[7] H. Fathabadi, "Novel wind powered electric vehicle charging station with vehicle-to-grid (V2G) connection capability," *Energy Convers. Manage.*, vol. 136, pp. 229–239, 2017.

[8] A. R. Hota, M. Juvvanapudi, and P. Bajpai, "Issues and solution approaches in PHEV integration to the smart grid," *Renew. Sustain. Energy Rev.*, vol. 30, pp. 217–229, 2014.

[9] Y. Mou, H. Xing, Z. Lin, and M. Fu, "Decentralized optimal demand-side management for PHEV charging in a smart grid," *IEEE Trans. Smart Grid*, vol. 6, no. 2, pp. 726–736, Mar. 2015.

[10] L. C. Casals, A. M. S. Gonzalez, B. Garcia, and J. Llorca, "PHEV battery aging study using voltage recovery and internal resistance from onboard data," *IEEE Trans. Veh. Technol.*, vol. 65, no. 6, pp. 4209–4216, Jun. 2016.

[11] H. Fathabadi, "High thermal performance Lithium-ion battery pack including hybrid active-passive thermal management system for using in hybrid/electric vehicles," *Energy*, vol. 70, pp. 529–538, 2014.

[12] N. Xue, W. Du, T. A. Greszler, W. Shyy, and J. R. R. A. Martins, "Design of a lithium-ion battery pack for PHEV using a hybrid optimization method," *Appl. Energy*, vol. 115, pp. 591–602, 2014.

[13] C. G. Hochgraf, J. K. Basco, T. P. Bohn, and I. Bloom, "Effect of ultracapacitor-modified PHEV protocol on performance degradation in lithium-ion cells," *J. Power Sources*, vol. 246, pp. 965–969, 2014.

[14] B. Zhao, Y. Shi, and X. Dong, "Pricing and revenue maximization for battery charging services in PHEV markets," *IEEE Trans. Veh. Technol.*, vol. 63, no. 4, pp. 1987–1993, May 2014.

[15] H. Zeng, S. Yang, and F. Z. Peng, "Design consideration and comparison of wireless power transfer via harmonic current," *IEEE Trans. Power Electron.*, vol. 32, no. 8, pp. 5943–5952, Aug. 2017.

[16] J. Deng, C. C. Mi, R. Ma, and S. Li, "Design of LLC resonant converters based on operation-mode analysis for level two PHEV battery chargers," *IEEE/ASME Trans. Mechatron.*, vol. 20, no. 4, pp. 1595–1606, Aug. 2015.

[17] M. Peng, L. Liu, and C. Jiang, "A review on the economic dispatch and risk management of the large-scale plug-in electric vehicles (PHEVs)-penetrated power systems," *Renew. Sustain. Energy Rev.*, vol. 16, no. 3, pp. 1508–1515, 2012.

[18] Z. Fan, "A distributed demand response algorithm and its application to PHEV charging in smart grids," *IEEE Trans. Smart Grid*, vol. 3, no. 3, pp. 1280–1290, Sep. 2012.

[19] H. Fathabadi, "Novel battery/photovoltaic hybrid power source for plug-in hybrid electric vehicles," *Solar Energy*, vol. 159, pp. 22–31, 2018.

[20] H. Fathabadi, "Novel fast dynamic MPPT (maximum power point tracking) technique with the capability of very high accurate power tracking," *Energy*, vol. 94, pp. 466–475, 2016.

[21] H. Fathabadi, "Novel high efficiency DC/DC boost converter for using in photovoltaic systems," *Solar Energy*, vol. 125, pp. 22–31, 2016.

Hassan Fathabadi was born in Tehran in 1969. He received the B.S., M.S., and Ph.D. degrees in electrical engineering from Tehran Polytechnic University, Tehran, Iran, in 1992, 1997, and 2002, respectively.

From 2009 to 2012, he was a Postdoctoral Researcher with the National Technical University of Athens, Athens, Greece, where he is currently an Associate Professor. He is the sole author of more than 65 papers published in high-ranking ISI journals and 23 inventions. His research interests include power electronics, microelectronics, control, mechatronics, and energy and power systems.